Electronic Supplementary Material (ESI) for Physical Chemistry Chemical Physics.
This journal is © the Owner Societies 2018

Supporting information

Pinpointing the active species of the Cu(DAT) catalyzed oxygen reduction reaction

Bas van Dijk[a], Jan P. Hofmann[b], and Dennis G. H. Hetterscheid[a*]

[a]Leiden Institute of Chemistry, Leiden University, 2300 RA Leiden, The Netherlands
[b]Laboratory of Inorganic Materials Chemistry, Department of Chemical Engineering and Chemistry, Eindhoven University of Technology, P.O. Box 513, 5600 MB Eindhoven, The Netherlands

Table of contents

1. Long-term stability of a Cu(DAT) solutions 2
2. EPR of Cu(DAT) powder 3
3. pH titrations on Cu(DAT) 4
4. Copper and DAT titrations followed by UV-Vis spectroscopy 6
5. Influence of MES buffer on Cu(DAT) 8
6. Electrochemical Quartz Crystal Microbalance experiments 9
7. Cyclic voltammetry in the presence of Cu(DAT) with gold and pyrolytic graphite electrodes 12
8. Koutecky-Levich analysis 14
9. XPS analysis of C 1s and N 1s regions of modified gold and pyrolytic graphite electrodes 16
10. Influence of DAT on the ORR activity of copper electrodes 18
11. RRDE and XPS experiments of Vulcan|Cu(DAT) 21
12. References 25

1. Long-term stability of a Cu(DAT) solutions

The stability of a **Cu(DAT)** solution was monitored by UV-Vis over time (Figure S1). Before the first spectrum was taken, two solutions were prepared: a 5 ml 0.1 M $NaClO_4$ solution containing 13.2 mM $Cu(OTf)_2$ and 5 ml of a 0.1 M $NaClO_4$ solution containing 13.2 mM 3,5-diamino-1,2,4-triazole (DAT). These solutions were mixed and within a minute, the first UV-Vis spectrum was taken. Slowly, the absorption at 380 nm was observed to increase. After 10.75 hours, the absorption at 380 nm reached a maximum and the absorption between 600 and 1000 nm had shifted. In addition, precipitation had formed in the solution. In the following hours, the absorption at 380 nm was found to decrease. Clearly, the **Cu(DAT)** solution is not stable over long periods of time. Therefore, all experiments were performed within 0-4 hours after preparation of the **Cu(DAT)** solution when only minor changes are observed in the UV-Vis spectrum.

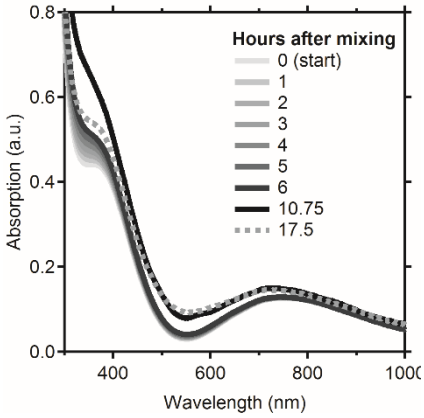

Figure S1. UV-Vis spectra recorded over the course of 17.5 hours of a 0.1 M $NaClO_4$ solution containing 6.6 mM of a 1:1 mixture of $Cu(OTf)_2$ and DAT. The evolution in time is illustrated with the color change from light grey to black. The grey dotted line represents the spectrum after 17.5 hours.

2. EPR of Cu(DAT) powder

A **Cu(DAT)** powder was obtained by removing water under reduced pressure of a 6.6 mM aqueous solution of a 1:1 mixture of $Cu(OTf)_2$ and DAT. Electron paramagnetic resonance (EPR) spectroscopy (Figure S2) was employed to check whether the powder agrees upon the structure of **Cu(DAT)** in solution. A broad peak at g = 2.16 was observed as well as the weak signal for the forbidden $M_s = \pm 2$ transition both indicating the presence of the dinuclear $Cu_2(\mu\text{-DAT})_2$ core. This confirms that the **Cu(DAT)** powder that was used for XPS analysis has the same electronic structure as the **Cu(DAT)** complex in solution.

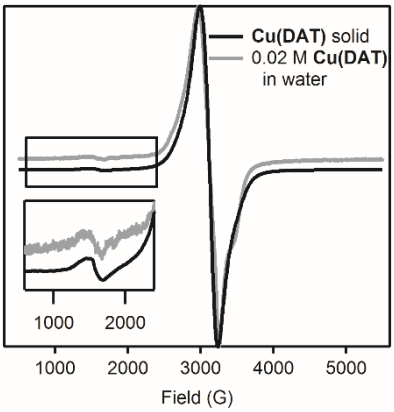

Figure S2. In black, the normalized EPR spectrum of the **Cu(DAT)** powder depicted. The spectrum was obtained at 9.35 GHz at 77 K. For comparison, the normalized EPR spectrum of **Cu(DAT)** in water (Figure 2) is depicted in grey. The inset depicts a zoom of the spectrum between 600 and 2400 Gauss.

3. pH titrations on Cu(DAT)

pH titrations were performed to study the influence of the pH on the complex as the triazole ligand might be protonated (pK_a of $HDAT^+$ is 4.4) or deprotonated (pK_a of DAT is 12.1).[1-3] An acidic titration on a 0.1 M $NaClO_4$ solution containing 30 mM of a 1:1 mixture of $Cu(OTf)_2$ and DAT was performed with 1.0 M $HClO_4$ (Figure S3a). A perchlorate solution was used in order to resemble the conditions of electrochemical measurements. At the inflection point, 2.1 equivalents of acid with respect to $Cu_2(\mu\text{-DAT})_2$ are transferred. This equals 1.05 equivalents with respect to the ligand DAT. At the inflection point, both of the coordinated DAT ligands of the $Cu_2(\mu\text{-DAT})_2$ core are protonated simultaneously with an estimated pK_a value of 3.5. The drop in pH is accompanied by a color change from green to light blue. The UV-Vis spectrum of **Cu(DAT)** at pH 4.8 has two distinct absorptions at 380 nm and circa 740 nm (Figure S3b). This latter signal has shifted to circa 800 nm in the UV-Vis spectrum upon acidification of the **Cu(DAT)** solution to pH 1 using $HClO_4$. Simultaneously, the distinctive absorption at 380 nm almost completely disappeared. The UV-Vis spectrum of **Cu(DAT)** at pH 1 was found to be qualitatively identical to the UV-Vis spectrum of $Cu(OTf)_2$ in absence of DAT.

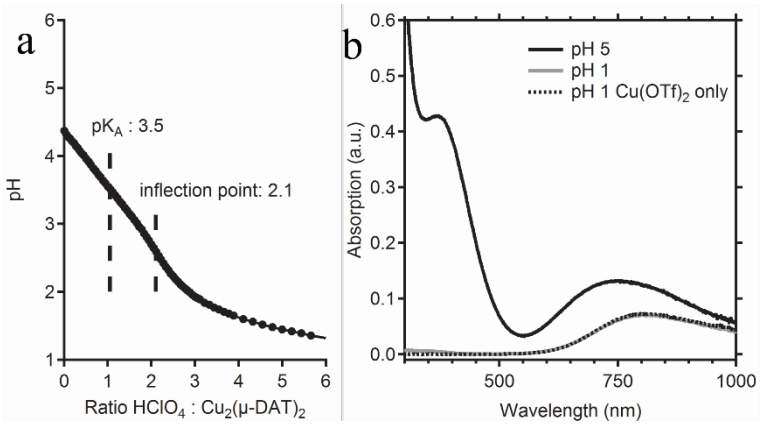

Figure S3. (a) shows the pH titration with 1.0 M $HClO_4$ of a 0.1 M $NaClO_4$ solution containing 30 mM of a 1:1 mixture of $Cu(OTf)_2$ and DAT with 1.0 M $HClO_4$. The ratio is given with respect to the dinuclear $Cu_2(\mu\text{-DAT})_2$ core. (b) shows the UV-Vis spectrum of a 0.1 M $NaClO_4$ solution containing 6.6 mM of a 1:1 mixture of $Cu(OTf)_2$ and DAT (pH 5, black solid line). Also depicted are the spectra of a 0.1 M $HClO_4$ solution (pH 1) containing either 6.6 mM of a 1:1 mixture of $Cu(OTf)_2$ and DAT (grey solid line) or only 6.6 mM $Cu(OTf)_2$ (black dotted line).

Starting from a 15 mM solution of a 1:1 mixture of $Cu(OTf)_2$ and DAT a titration with 1.1 M NaOH was performed under continuous stirring (Figure S4). Small amounts of green precipitation were observed to form above pH 5.5 and increased in quantity as the pH further increased. At circa pH 12 a turbid solution was obtained. The titration with NaOH was stopped and immediately followed by a back titration with 1.0 M $HClO_4$. The back titration showed hysteresis around the inflection point. Moreover, the precipitation slowly disappeared while the pH was lowered and eventually a clear solution was obtained below pH 5. The observed hysteresis around the inflection point indicates that an additional process coupled to a deprotonation takes place. A coordinating H_2O is most likely deprotonated as one equivalent of NaOH is required to reach the inflection point. As a result, the anionic hydroxyl is now

able to form an intermolecular bridge between complexes. Ultimately, this can lead to the formation of insoluble coordination polymers, which are frequently observed in case of aqueous copper complexes.[4-6]

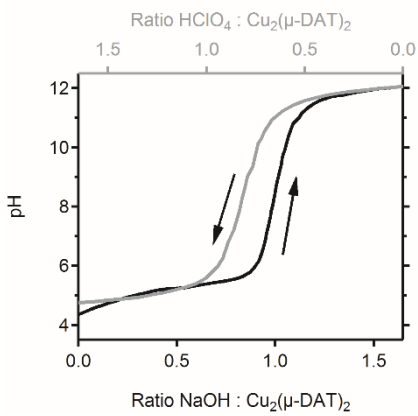

Figure S4. pH titration of an aqueous 15 mM solution of a 1:1 mixture of $Cu(OTf)_2$ and DAT with 1.1 M NaOH (black line, bottom axis) and the back-titration with 1.0 M $HClO_4$ (grey line, top axis). The ratio is given with respect to the dinuclear $Cu_2(\mu\text{-DAT})_2$ core.

4. Copper and DAT titrations followed by UV-Vis spectroscopy

In order to investigate the influence of different ligand to copper ratios, two titrations were performed in 0.1 M $NaClO_4$. First, 10 µL aliquots of a solution containing 0.42 M $Cu(OTf)_2$, 6.6 mM DAT, and 0.1 M $NaClO_4$ were added to a 2.5 ml solution of 6.6 mM DAT in 0.1 M $NaClO_4$. UV-Vis spectra were recorded after every addition (Figure S5). As soon as $Cu(OTf)_2$ was added, the characteristic absorption at 380 nm as well as a broad absorption with a maximum at 720 nm corresponding to the d-d transition of Cu^{II} started to appear. While the $Cu(OTf)_2$ concentration was increased, the absorption at 380 nm increased and sharpened. Moreover, the d-d absorption not only increases but also shifts to 780 nm. The latter event is an indication for a change in ligand environment as this affects the d-d transition. An opposite shift is observed when a 0.42 M DAT solution containing 6.6 mM $Cu(OTf)_2$ and 0.1 M $NaClO_4$ is titrated to a 6.6 mM $Cu(OTf)_2$ solution in 0.1 M $NaClO_4$ (Figure S6). In this case, the d-d band shifts to lower wavelengths most likely due to a larger ratio of coordinated DAT with respect to copper. The absorption at 380 nm quickly increases in intensity but is eventually overlapped by a large absorption in the UV area.

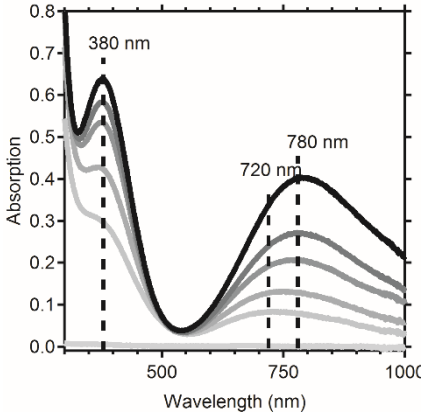

Figure S5. UV-Vis spectra of the titration of $Cu(OTf)_2$ to a 6.6 mM DAT solution in 0.1 M $NaClO_4$. In the order of increasing darkness are depicted the spectra of 0, 0.5, 1, 2, 3 and 4 equivalents of $Cu(OTf)_2$ with respect to DAT.

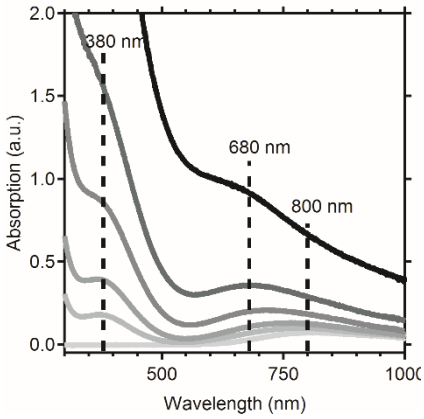

Figure S6. UV-Vis spectra of the titration of DAT to a 6.6 mM $Cu(OTf)_2$ solution in 0.1 M $NaClO_4$. In the order of increasing darkness are depicted the spectra of 0, 0.5, 1, 2, 3 and 4 equivalents of DAT with respect to $Cu(OTf)_2$.

Titrations were also performed at pH 1 to see the effect of protonated DAT (Figures S7 and S8). When $Cu(OTf)_2$ was titrated to a DAT solution in 0.1 M $HClO_4$, the absorption corresponding to the d-d absorption increased in intensity but did not shift (Figure S7). The maximum was found at 800 nm which corresponds to a $Cu(OTf)_2$ only solution at pH 1 (Figure S3). A slight absorption can be observed at 355 nm but only becomes significant when the amount of DAT was increased up to 11 equivalents with respect to $Cu(OTf)_2$ (Figure S8). This indicates that an infinite small amount of $HDAT^+$ still coordinates but hardly has a change on the ligand environment of copper, as the d-d transition at 800 nm does not shift nor changes in intensity.

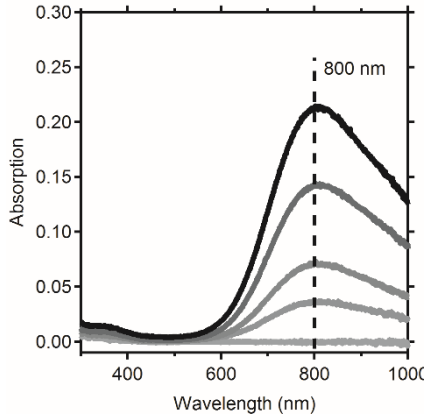

Figure S7. UV-Vis spectra of the titration of $Cu(OTf)_2$ to a 6.6 mM DAT solution in 0.1 M $HClO_4$. In the order of increasing darkness are depicted the spectra of 0, 0.5, 1, 2, and 3 equivalents of $Cu(OTf)_2$ with respect to DAT.

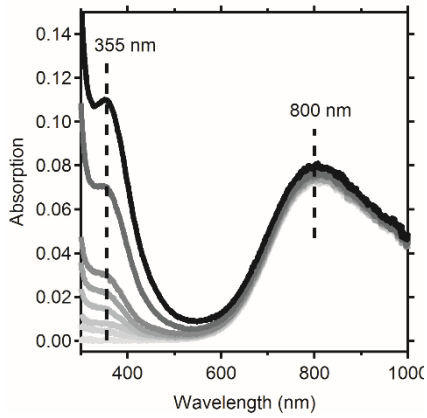

Figure S8. UV-Vis spectra of the titration of DAT to a 6.6 mM $Cu(OTf)_2$ solution in 0.1 M $HClO_4$. In the order of increasing darkness are depicted the spectra of 0, 0.5, 1, 2, 3, 4, 8 and 11 equivalents of DAT with respect to $Cu(OTf)_2$.

5. Influence of MES buffer on Cu(DAT)

It was found that the combination of **Cu(DAT)** and a phosphate or Britton-Robinson buffer led to precipitation of **Cu(DAT).** Hence, 0.03 M of 2-(*N*-morpholino)ethanesulfonic acid (MES) was investigated as a buffer, since it has a pK_a of 6.15 and thus a useful buffering range close to pH 4.8.[7,8] Moreover, no immediate precipitation was observed in combination with **Cu(DAT)**. Although it has been reported that MES is not likely to coordinate to Cu^{II},[9] a deviation in the UV-Vis spectrum was observed implying that some coordination of MES does take place (Figure S9). The absorption belonging to the d-d transition shifts while the absorption at 380 nm increases significantly. Coordination can be expected for a complex such as **Cu(DAT)** with labile ligands in the coordination sphere but the $Cu_2(\mu\text{-DAT})_2$ core remains intact as illustrated by the 380 nm absorption and the identical EPR spectra of **Cu(DAT)** in the presence and absence of MES (Figure S10).

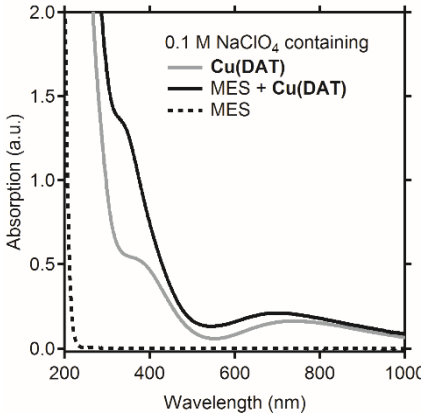

Figure S9. The UV-Vis spectra of a 0.1 M $NaClO_4$ solution with 6.6 mM of a 1:1 mixture of $Cu(OTf)_2$ and DAT (**Cu(DAT)**, grey solid line), 0.03 M MES buffer (dotted black line) and a mixture of both (solid black line).

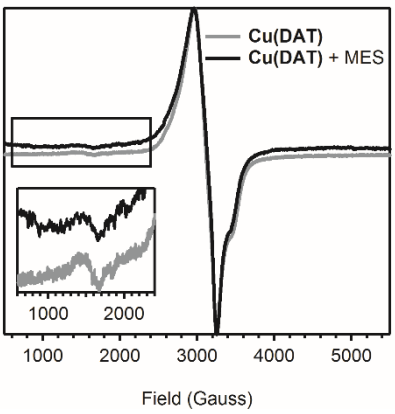

Figure S10. In grey, the normalized EPR spectrum of a 6.6 mM **Cu(DAT)** solution (Figure 2, taken at 9.36 GHz) is shown. The black lines show the normalized EPR spectrum of 6.6 mM **Cu(DAT)** + 0.03 M MES (taken at 9.34 GHz. The inset shows a zoom of the spectrum between 600 and 2400 Gauss. Both spectra were taken at 77 K.

6. Electrochemical Quartz Crystal Microbalance experiments

For the sensitive microbalance experiments a sensitivity coefficient relating the frequency to mass can be determined by the electrodeposition of Pb^0 as is described elsewhere.[10] However, frequency changes might not solely depend on mass changes as for example the viscoelasticity and surface roughness of the deposition also have an effect on the frequency.[11]

A separate electrochemical quartz crystal microbalance (EQCM) measurement was performed for a solution containing 6.6 mM of only DAT. In the potential window of 0.0 to 1.0 V an anodic peak is observed during cyclic voltammetry (CV) accompanied by a negligible frequency change. When the potential window is broadened to 1.2 V it becomes clear that the oxidation that has an onset at 0.9 V *versus* the reversible hydrogen electrode (RHE) is part of an oxidation that produces significant currents above 1.0 V (Figure S11). The initial positive sweep is followed by a negative sweep where a broad reductive peak between 0.9 and 0.4 V *versus* RHE can be observed. Accordingly, the oxidation starting at 0.9 V is linked to the oxidation of DAT but does not lead to signification deposition.

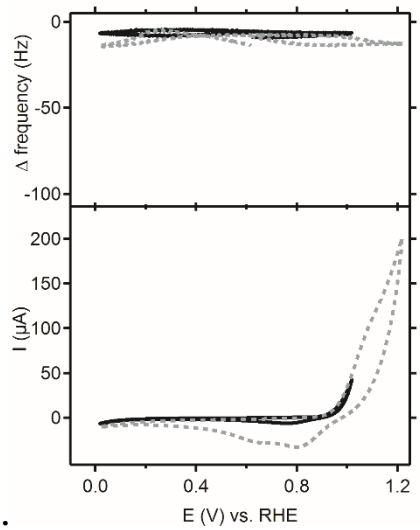

Figure S11. A cyclic voltammogram combined with a quartz crystal microbalance experiment of a 0.1 M $NaClO_4$ solution (pH 4.4) containing 6.6 mM DAT measured at a 10 mV/s scan rate. The voltammograms were recorded between 0 and 1 V (solid black line) or 1.3 V (dotted grey line).

The electrochemical deposition of material by **Cu(DAT)** can also be induced by chronoamperometry. Applying a fixed potential of 0.2 V on a gold electrode induces a steady decrease of frequency, thus increase of mass, of the electrode (Figure S12). Figure S13 shows that the ORR activity of the electrodeposition induced by chronoamperometry (^{CA}Au|**Cu(DAT)**) shows the same current profile on gold as the deposition generated by cyclic voltammetry (^{CV}Au|**Cu(DAT**, 30 cycles between 0 and 1 V at 100 mV/s). Also, for both ^{CV}Au|**Cu(DAT)** and ^{CA}Au|**Cu(DAT)** the activity increases by circa 30% in the course of 40 scans. The difference in absolute current might be caused by the difference in the amount of deposited material. During modification with cyclic voltammetry, part

of the deposition is stripped above 0.8 V whereas during chronoamperometry the potential is held at 0.2 V.

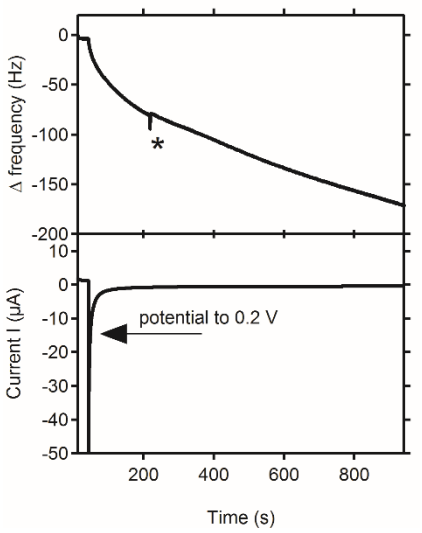

Figure S12. A quartz crystal microbalance experiment combined with chronoamperometry. A gold electrode in a 0.1 M $NaClO_4$ (pH 4.8) solution containing 6.6 mM of a 1:1 mixture of $Cu(OTf)_2$ and DAT was modified by chronoamperometry. For the first 30 seconds, the potential was held at 0.8 V. Next, the potential was set at 0.2 V for 15 minutes. The current response is displayed in the bottom panel while the corresponding frequency change is displayed in the top panel. The asterisk (*) depicts an artifact.

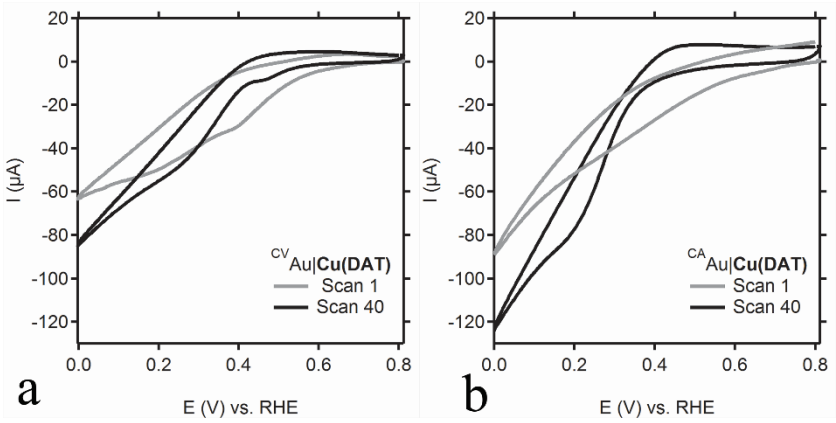

Figure S13. Cyclic voltammograms at a scan rate of 100 mV/s of modified gold electrodes in an oxygen-purged 0.03 M MES buffer in a 0.1 M $NaClO_4$ solution (pH 5.2). The electrodes were either pre-modified by cyclic voltammetry (a) or chronoamperometry (b) in a **Cu(DAT)** solution. For clarity, only the first (light grey) and last (40th, black) scans are shown.

The deposition formed by **Cu(DAT)** can readily be stripped off by performing CV in a potential window up to 1.3 V (Figure S14). A gold electrode was modified by repeated CV scans in an 0.1 M $NaClO_4$ electrolyte containing **Cu(DAT)**. The EQCM measurement shows that the intensity of the oxidative peak at 0.8 *versus* RHE drastically increases above 1.0 V and is accompanied by a severe decrease in mass indicating loss of material. Subsequent scanning in this broader potential window shows that deposition formed in the cathodic region is readily stripped above 1.0 V so build-up of material on the electrode does not take place anymore.

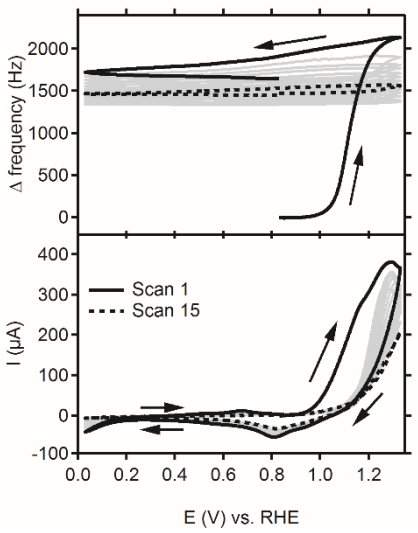

Figure S14. Stripping of the deposition of a modified gold electrode in a 0.1 M $NaClO_4$ (pH 4.8) solution containing 6.6 mM of a 1:1 mixture of $Cu(OTf)_2$ and DAT by EQCM combined with cyclic voltammetry at a 10 mV/s scan rate. The material was deposited on the electrode by performing CV for 15 scans between 0 and 1 V at a 10 mV/s scan rate in the same electrolyte prior to stripping.

7. Cyclic voltammetry in the presence of Cu(DAT) with gold and pyrolytic graphite electrodes

A gold disk electrode was modified using the same procedure as the EQCM experiments were performed: a CV was taken in a 6.6 mM solution of a 1:1 ratio of $Cu(OTf)_2$ and DAT in a 0.1 M $NaClO_4$ electrolyte solution. 30 cycles at a 100 mV/s scan rate were performed to obtain the modified electrode ^{CV}Au|**Cu(DAT)**. Compared to unmodified gold, the onset is at slightly higher potentials and larger currents are acquired. Also, the ring shows less current implying better selectivity. However, the activity drops over repetitive scanning. Most likely, the deposition cannot bind strong enough on gold to perform rotating ring disk electrode (RRDE) experiments with high rotation rates. In contrast, when a stationary gold electrode is used, the activity increases upon repetitive potential cycling (Figure S13 and S18) similar to the behavior of PG|**Cu(DAT)** (Figure 4). As gold is active in the same potential window for the ORR (Figure S15), any attributions to active species cannot be made unambiguously when gold is used. Therefore, pyrolytic graphite (PG) was used as electrode as it shows qualitatively the same electrochemistry for **Cu(DAT)** as with gold (Figure S16).

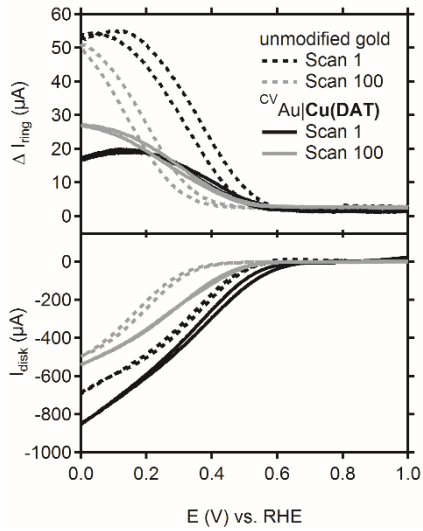

Figure S15. RRDE experiment with a gold disk electrode (0.196 cm^2) in an oxygen-purged 0.1 M $NaClO_4$ solution containing 0.03 M MES buffer (pH 5.2). The cyclic voltammogram of the gold disk which was rotated at 2000 rpm (bottom panel) and the current response of the platinum ring that was set at a potential of 1.2 V (top panel) are depicted. The dotted lines correspond to an unmodified gold disk while the solid lines correspond to the modified electrode ^{CV}Au|**Cu(DAT)**. In black, the first scan is shown while the grey lines show the last (100th) scan. The CV was taken at a 100 mV/s scan rate.

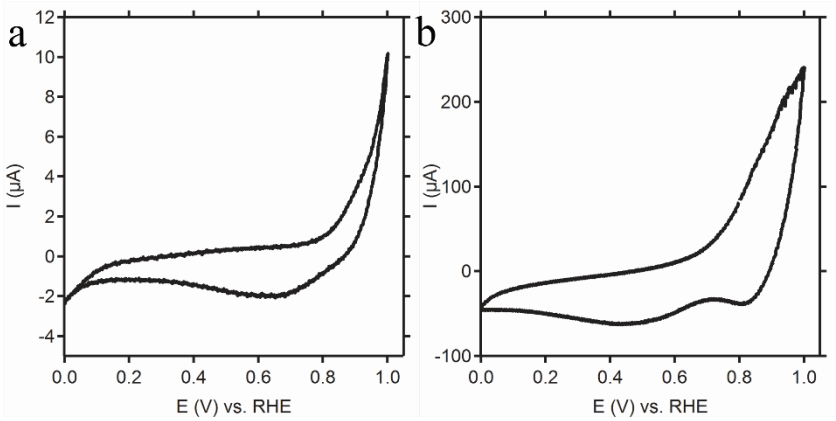

Figure S16. Cyclic voltammograms that are recorded at a 25 mV/s scan rate in a 0.1 M $NaClO_4$ (pH 4.8) solution with 6.6 mM of a 1:1 ratio of $Cu(OTf)_2$ and DAT with (a) gold and (b) pyrolytic graphite (PG) working electrodes.

8. Koutecky-Levich analysis

The linear fits in Figure S17a show that the limiting current for dioxygen reduction at different rotation rates behaves according to the Koutecky-Levich equation[12]:

$$\frac{1}{I} = \frac{1}{I_k} + \frac{1}{I_L} \tag{1}$$

where I is the observed current, I_k is the kinetically controlled current that would be observed when the mass transport rate to the electrode would be much greater than the reaction rate and I_L is the diffusion-limited current that would be observed when the rate of the reaction is much greater than the mass transport rate. The diffusion-limited current can in turn be described by the Levich equation:

$$I_L = 0.62nFAD_O^{2/3}C_O\,\nu^{-1/6}\omega^{1/2} = BnA\omega^{1/2} \tag{2}$$

where n corresponds to the number of transferred electrons, F is the Faraday constant (C/mol), A is the electrode area (cm^2), D_O is the diffusion coefficient of O_2 (cm^2/s), C_O is the concentration of O_2 in the electrolyte, ν is the kinematic viscosity (cm^2/s) and ω the rotation rate (rad/s). As most of these are constants, the equation can be simplified with the Levich constant defined as B. This constant was determined by performing rotating ring disk electrode (RRDE) experiments with a platinum disk electrode, as platinum is known to be a 4-electron dioxygen reduction catalyst. B can be calculated using the slope of the Koutecky-Levich plot as the following equation holds:[13]

$$slope = \frac{1}{BnA} \tag{3}$$

For the platinum electrode the slope, n (4) and A (0.196 cm^2) are known, so B could be determined and used to calculate n for the modified PG electrode for which A (0.12 cm^2) and the slope are known as well. n was calculated to be 1.2 indicating that dioxygen is reduced to mainly superoxide and partly peroxide species.

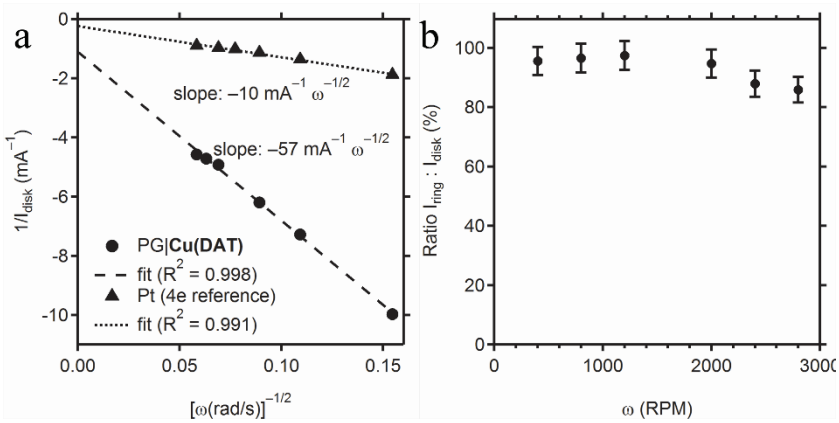

Figure S17. (a) shows the Koutecky-Levich plot of the inverse of the average limiting current between 0.40-0.42 V of PG|**Cu(DAT)** (rounds, Figure 4b) versus the inverse square root of the rotation rate and the result of a linear fit. Also shown is the inverse of the average limiting current between 0.30 and 0.35 V for a Pt disk electrode (triangles) used as calibration for the Levich equation in oxygen-saturated 0.1 M NaOH. (b) shows the ratio of the average limiting current of the ring to the average limiting current of PG|**Cu(DAT)** between 0.40 and 0.42 V versus the rotation speed in 0.1 M NaOH. The ratio was corrected for the collection efficiency (22%) of the ring that was determined with the $[Fe(CN)_6]^{4-}/[Fe(CN)_6]^{3-}$ redox couple.

9. XPS analysis of C 1s and N 1s regions of modified gold and pyrolytic graphite electrodes

For X-ray photoelectron spectroscopy (XPS) analysis, the following procedures were followed to obtain ^{CV}Au|**Cu(DAT)** and ^{CA}Au|**Cu(DAT)**. EQCM gold electrodes were used in a similar set-up as the EQCM experiments. Sample ^{CV}Au|**Cu(DAT)** was prepared with cyclic voltammetry by performing 30 CV scans between 0 and 1 V at a 100 mV/s scan rate in a 0.1 M $NaClO_4$ solution containing 6.6 mM of a 1:1 ratio of $Cu(OTf)_2$ and DAT at pH 4.8. Sample ^{CA}Au|**Cu(DAT)** was prepared potentiostatically by applying 0.2 V for 15 minutes. The whole set-up was stationed in a glove bag under an N_2 atmosphere to prevent contact with air upon removal of the electrode from the EQCM cell. The electrodes were rinsed with Ar purged water and dried under high vacuum before XPS analysis.

^{Cat}Au|**Cu(DAT)** was prepared with cyclic voltammetry by performing 30 CV scans between 0 and 1 V at a 100 mV/s scan rate in a 0.1 M $NaClO_4$ solution containing 6.6 mM of a 1:1 ratio of $Cu(OTf)_2$ and DAT at pH 4.8. Next, the electrode was put in an oxygen-saturated 0.03 M MES buffer (pH 5.2) in 0.1 M $NaClO_4$. 100 CV cycles between 0 and 1 V at a 100 mV/s scan rate were performed. The ORR onset was observed to increase after repetitive scanning up to 100 scans (Figure S18) as was also observed with RRDE experiments on PG|**Cu(DAT)**.

PG|**Cu(DAT)** was prepared in a regular electrochemical set-up by performing 90 CV scans between 0 and 1 V at a 100 mV/s scan rate in a 0.1 M $NaClO_4$ solution containing 6.6 mM of a 1:1 ratio of $Cu(OTf)_2$ and DAT at pH 4.8. 90 instead of 30 CV scans were used to increase the intensity of the XPS signal. The electrode was rinsed with N_2 purged water and dried under high vacuum. Care was taken to prevent contact with air during handling and transferring the electrode into the XPS apparatus.

Next, XPS analysis was performed on all samples (Figure S19). Also, carbon to copper ratios are given in Table S1.

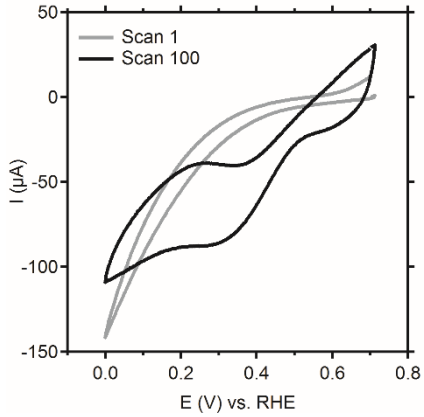

Figure S18. Cyclic voltammogram of ^{Cat}Au|**Cu(DAT)** directly after the modification in an oxygen purged 0.1 M $NaClO_4$ solution containing 0.03 M MES buffer at a pH of 5.2. 100 cycles at a 100 mV/s scan rate were performed.

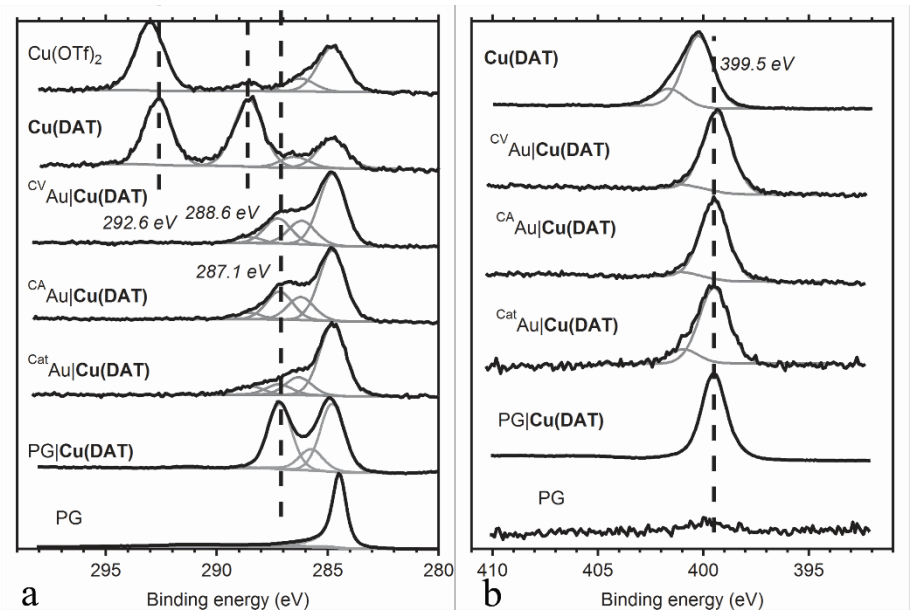

Figure S19. (a) C 1s and (b) N 1s XPS spectra (black lines) of the modified electrodes ^{CV}Au|**Cu(DAT)**, ^{CA}Au|**Cu(DAT)**, ^{Cat}Au|**Cu(DAT)**, PG|**Cu(DAT)** and the reference compounds **Cu(DAT)**, $Cu(OTf)_2$ and PG electrode. In grey, the deconvolution is depicted.

Table S1. The ratio of several carbon species with respect to the total amount of copper of the modified electrodes ^{CV}Au|**Cu(DAT)**, ^{CA}Au|**Cu(DAT)**, ^{Cat}Au|**Cu(DAT)** and the reference compounds **Cu(DAT)** and $Cu(OTf)_2$ as determined by XPS.

Elemental ratio	Corresponding carbon species (eV)[a]	$Cu(OTf)_2$	**Cu(DAT)**	^{CV}Au|**Cu(DAT)**	^{CA}Au|**Cu(DAT)**	^{Cat}Au|**Cu(DAT)**
C : Cu	293.0 (OTf^-)	1.6				
	292.6 (OTf^-)		2.0			
	288.6 (DAT)		2.2			
	286.2			1.1	1.2	
	287.2			1.4	1.2	
	288.5			0.3	0.3	
	286.4					1.9
	287.7					1.1
	289.1					0.7

[a]The ratio of the carbon species at 284.8 eV is omitted as this mostly corresponds to adventitious carbon for these samples.

10. Influence of DAT on the ORR activity of copper electrodes

To study the electrochemical effect of DAT on a copper surface, a copper disk was modified by cyclic voltammetry similar to the modification of PG to obtain PG|**Cu(DAT)**. A copper disk electrode was modified by cyclic voltammetry between 0 and 1 V *versus* RHE in a 0.1 M $NaClO_4$ solution containing 6.6 mM DAT to obtain Cu|DAT. Notably, oxidation of copper occurs above 0.5 V thus the scan rate was adjusted to 250 mV/s to reduce the corrosion time of the copper disk per cycle. The amount of scans was increased to 75 to maintain the same total modification time of 10 minutes. Figure S20 shows the ORR activity studied with RRDE experiments of Cu|DAT compared to PG|**Cu(DAT)**. Cu|DAT was studied at both pH 5.2 and pH 13. In both cases, the CV of the disk differs significantly from PG|**Cu(DAT)**. Also, the shape of the CV of Cu|DAT stabilized after repetitive CV cycling. Figure S21 shows a comparison of the ORR activity of Cu|DAT as compared to an unmodified copper disk electrode. At pH 5.2, the shape of the CV of Cu|DAT is more similar to copper than to PG|**Cu(DAT)** (Figure S20). However, the surface modification did lead to some differences in the CV of the disk. Furthermore, some ring current can be observed for Cu|DAT whereas unmodified copper does not show any ring current. At pH 13 the shape of the last CV of Cu|DAT and unmodified copper are more comparable than at pH 5.2.

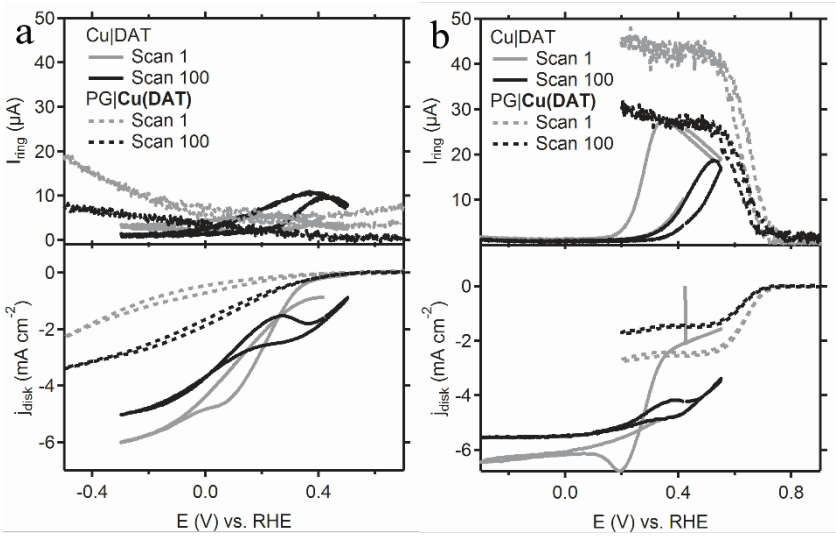

Figure S20. RRDE experiment of Cu|DAT in an oxygen-saturated electrolyte (solid line). Cu|DAT was studied in both (a) 0.03 M MES in 0.1 M $NaClO_4$ at pH 5.2 and (b) 0.1 M NaOH at pH 13. For comparison, the results of PG|**Cu(DAT)** (Figure 4) are depicted as well (dotted lines). Current densities are given for the disk as the surface from Cu|DAT (0.196 cm^2) is different from PG|**Cu(DAT)** (0.12 cm^2). The CV was taken at a 100 mV/s scan rate while the disk was rotated at 2000 RPM.

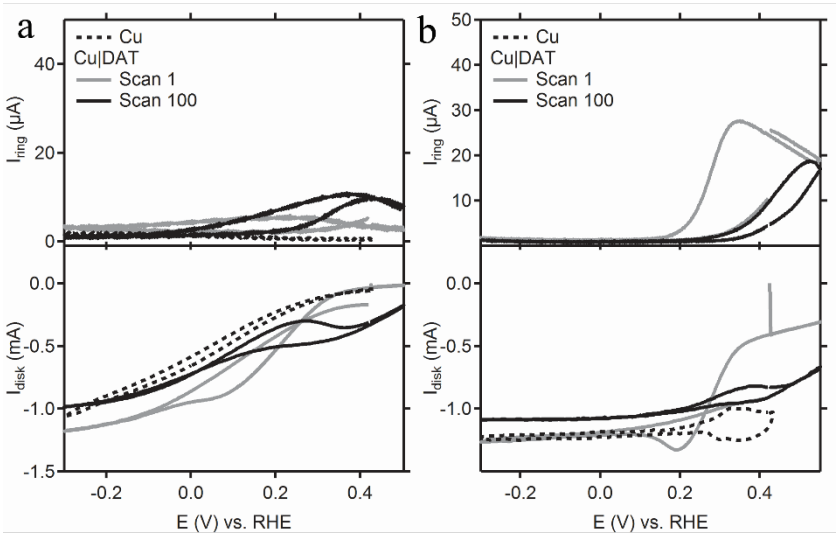

Figure S21. RRDE experiment with unmodified Cu (black dotted lines) and modified Cu|DAT disk electrodes (solid lines) in an oxygen-saturated electrolyte. Both the electrodes were studied in a (a) 0.03 M MES in 0.1 M $NaClO_4$ at pH 5.2 and (b) 0.1 M NaOH at pH 13. The CV was taken at a 100 mV/s scan rate while the disk was rotated at 2000 RPM. In (b) the ring current during the CV of the unmodified Cu disk was not monitored.

Possibly, the modified layer of Cu|DAT is quickly stripped off during the ORR experiments, because the shape of the CV of Cu|DAT resembles the CV of unmodified copper. Therefore, the ORR activity of unmodified copper was also studied in electrolytes containing 6.6 mM DAT at pH 5.2 and pH 13 (Figure S22) with RRDE. At both pH 5.2 and pH 13, the CV of the copper electrode did not change after repetitive potential cycling in contrast to the PG|**Cu(DAT)** electrode. Also, larger currents are observed in the case of the copper electrode. Experiments in combination with a ring could not be performed because DAT is oxidized above 0.9 V (Figure S11). Moreover, the copper electrode is oxidized above 0.5 V thus limiting the potential window wherein CV was performed. Notably, the solution slowly developed a yellow color in the course of the ORR experiments that were performed at pH 13. Most likely, DAT is slowly disintegrated due to the combination of electrochemistry and high pH. A pH 13 solution containing DAT not subjected to electrochemical measurements remained colorless.

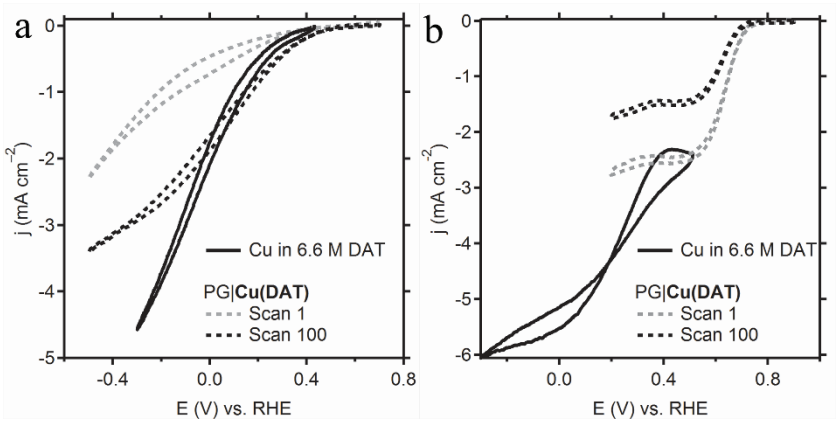

Figure S22. Rotating disk electrode experiments of a copper electrode (0.196 cm^2) in an oxygen-saturated electrolyte containing 6.6 mM DAT (black solid line). The copper electrode was studied in both (a) 0.03 M MES in 0.1 M $NaClO_4$ at pH 5.2 and (b) 0.1 M NaOH at pH 13. For comparison, the results obtained with PG|**Cu(DAT)** (Figure 4) are depicted as well (dotted lines). Current densities are given as the surface from PG|**Cu(DAT)** (0.12 cm^2) is different from the copper electrode (0.196 cm^2). The CV was taken at a 100 mV/s scan rate while the disk was rotated at 2000 RPM.

11. RRDE and XPS experiments of Vulcan|Cu(DAT)

Vulcan|**Cu(DAT)** was prepared according to the reported procedure[14] from DAT and $CuSO_4 \cdot 5H_2O$ (≥99.995 % trace metal basis, Sigma Aldrich) by mixing 1.00 g Vulcan XC-72R (Cabot) with 0.200 g $CuSO_4 \cdot 5H_2O$ (99.995%, Sigma Aldrich) in 20 ml water and sonicating the mixture for 2 hours to obtain a viscous suspension. Next, a solution of 0.159 g DAT in 10 ml water was added dropwise to the stirred suspension. After addition of DAT, the mixture was left stirring for an additional 20 hours. Subsequently, the black solids were collected through filtration. The remaining black paste was further dried in a vacuum oven at 90 °C for 3.5 hours. Following, the brittle solid was pulverized with pestle and mortar to obtain Vulcan|**Cu(DAT)** which was further analyzed by XPS (Figure S23 and S24).

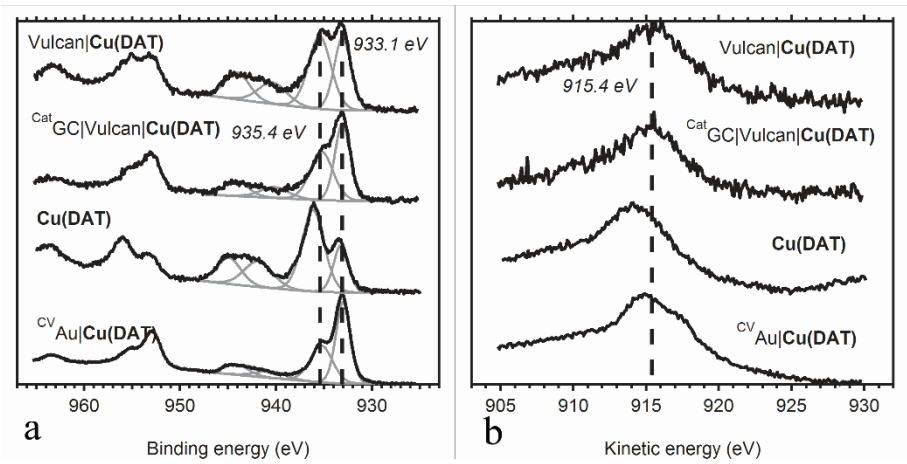

Figure S23. XPS spectra (black lines) of the modified electrodes ^{CV}Au|**Cu(DAT)** and ^{Cat}GC|Vulcan|**Cu(DAT)** and the reference compounds Vulcan|**Cu(DAT)** and **Cu(DAT)**. In grey, the deconvolution of the $Cu2p_{3/2}$ region is depicted. (a) shows the Cu 2p region of the spectra and (b) shows the Cu $L_3M_{4,5}M_{4,5}$ Auger spectra.

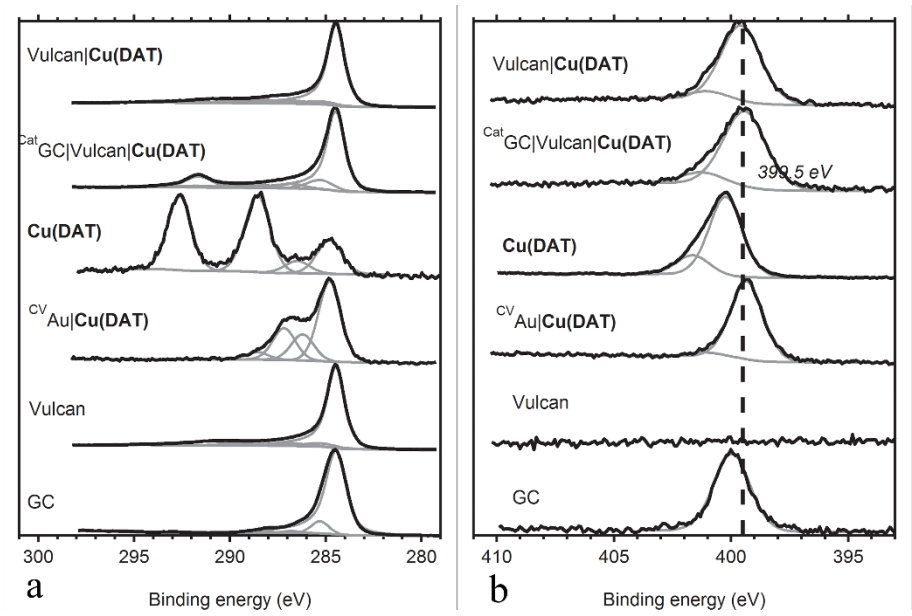

Figure S24. (a) C 1s and (b) N 1s XPS spectra (black lines) of the modified electrodes ^{CV}Au|**Cu(DAT)** and ^{Cat}GC|Vulcan|**Cu(DAT)** and the reference compounds **Cu(DAT)** and Vulcan|**Cu(DAT)** as well as bare GC and Vulcan. In grey, the deconvolution is depicted.

A GC disk electrode (0.196 cm^2) was modified by dropcasting Vulcan|**Cu(DAT)** on the electrode as previously reported.[14] The onset for oxygen reduction with GC|Vulcan|**Cu(DAT)** was found to correspond to the reported onset (Figure S25).[14] In addition, GC|Vulcan|**Cu(DAT)** was tested under the same conditions as PG|**Cu(DAT)** in a pH 5 MES buffer (Figure S26). GC|Vulcan|**Cu(DAT)** is clearly more active and seems to achieve limiting currents within the potential window. The 100th scan is displayed for both modified electrodes. For PG|**Cu(DAT)**, the 100th scan corresponds to the most active scan. For GC|Vulcan|**Cu(DAT)**, a minimal decrease in activity is observed over the course of 100 scans. These results indicate that the substrate plays an a very important role in the oxygen reduction activity.

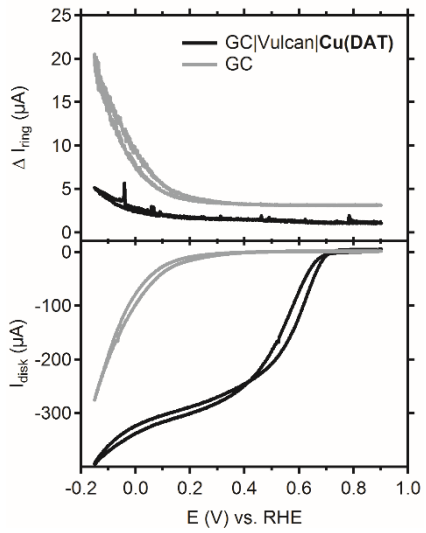

Figure S25. RRDE experiment of GC|Vulcan|**Cu(DAT)** disk in an oxygen-saturated pH 7 Britton-Robinson buffer in 0.1 M $NaClO_4$. The solid black lines depict the disk (bottom graph) and ring (top graph) current responses. The grey solid lines depict the current response when a freshly polished GC disk was used. The CV was performed at a 5 mV/s scan ate while the ring was set to 1.2 V and the disk rotated at 1600 rpm.

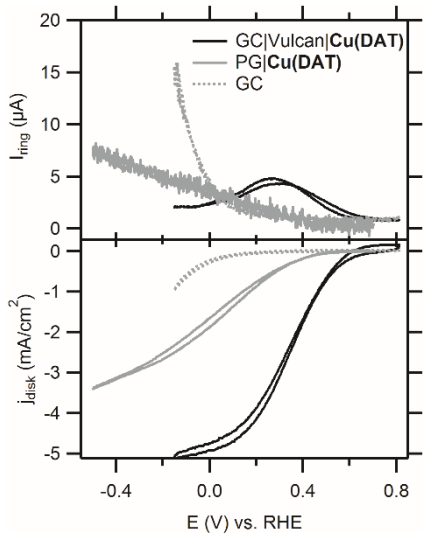

Figure S26. RRDE experiment of GC|Vulcan|**Cu(DAT)** disk (0.196 cm^2) in an oxygen-saturated pH 5.2 MES buffer in 0.1 M $NaClO_4$. The solid black lines depict the disk (bottom graph) and ring (top graph) current responses of the 100th scan. The grey dotted lines correspond to a freshly polished GC disk. The grey solid lines belong to the 100th scan of a PG|**Cu(DAT)** disk (0.12 cm^2. The CV was performed at a 100 mV/s scan ate while the ring was set to 1.2 V and the disk rotated at 2000 rpm.

Another GC electrode (0.07 cm^2) was modified by dropcasting Vulcan|**Cu(DAT)**. With this electrode (^{Cat}GC|Vulcan|**Cu(DAT)**), 103 CV cycles between 0.9 and 0 V at a 100 mV/s scan rate were performed in an oxygen purged pH 7 Britton-Robinson buffer in 0.1 M $NaClO_4$. After performing oxygen reduction, the electrode was rinsed with water and dried under a soft stream of air. XPS measurements were performed to analyze the composition of ^{Cat}GC|Vulcan|**Cu(DAT)** after catalysis (Figures S23 and S24). Within the Cu 2p region both ^{Cat}GC|Vulcan|**Cu(DAT)** and Vulcan|**Cu(DAT)** show similarities with ^{CV}Au|**Cu(DAT)** and ^{CA}Au|**Cu(DAT)**. Copper species with Cu $2p_{3/2}$ binding

energies of 933.1 and 935 eV are observed for all samples (Figure S23a). Also, the Auger parameter in the Cu $L_3M_{4,5}M_{4,5}$ spectrum has a kinetic energy of 915.4 eV for all species (Figure S23b). Two species are observed in the N 1s region for both Vulcan|**Cu(DAT)** and ^{Cat}GC|Vulcan|**Cu(DAT)** with BEs of 399.5 eV and 401.2 eV (Figure S24b). The (unpolished) GC electrode also contains a N 1s species, but this is different from Vulcan|**Cu(DAT)** species. Most importantly, the reference **Cu(DAT)** powder was found to differ from Vulcan|**Cu(DAT)** implying that the complex **Cu(DAT)** is not present in Vulcan|**Cu(DAT)** when it is prepared according to the literature procedure.[14] This is further supported by the (too) low nitrogen to copper ratio (Table 1). Moreover, the C 1s region is very different from **Cu(DAT)** and ^{CV}Au|**Cu(DAT)** (Figure S24a). This is due to the use of Vulcan and GC which are both carbon based materials and thus their strong signals overlap all other signals. Here, the most important species for both Vulcan|**Cu(DAT)** and ^{Cat}GC|Vulcan|**Cu(DAT)** is the graphitic sp^2 carbon with a BE of 284.5 eV. The carbon species with a BE of 291.6 eV in ^{Cat}GC|Vulcan|**Cu(DAT)** might correspond to the π-π* transition shake-up of graphite and does not correspond to **Cu(DAT)**. Also, the carbon composition is different compared to ^{cv}Au|**Cu(DAT)**.

The negligible change of the copper composition between Vulcan|**Cu(DAT)** and ^{Cat}GC|Vulcan|**Cu(DAT)** and the large resemblance with ^{CV}Au|**Cu(DAT)** indicate that most of the catalytic active sites of Vulcan|**Cu(DAT)** have not performed ORR due the diffusion limitation of oxygen. Figure S27 shows the corresponding CV response. Clearly, most of the oxygen near the catalytic surface has been reduced in only the first scan as the following scans show a far lower current response. Purging the electrolyte after scan 3 with O_2 for a brief moment did lead to a slight increase of ORR current in the first following scan.

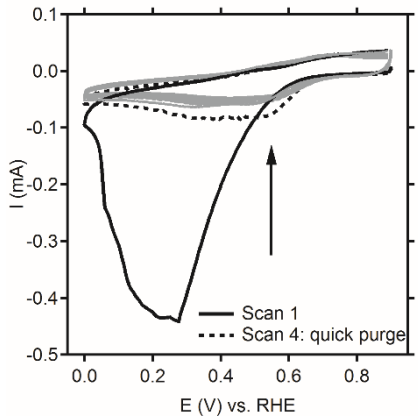

Figure S27. ORR response of ^{Cat}GC|Vulcan|**Cu(DAT)** that was analyzed by XPS hereafter. CV was performed between 0.9 and 0 V for 103 cycles with a scan rate of 100 mV/s in a pH 7 Britton-Robinson buffer in 0.1 M $NaClO_4$. After scan 3, the potential cycling was halted to re-purge the electrolyte with O_2 before continuing the potential cycling.

12. References

1. L. Antolini, A. C. Fabretti, D. Gatteschi, A. Giusti and R. Sessoli, *Inorg. Chem.*, 1991, **30**, 4858–4860.
2. A. C. Fabretti, *J. Crystallogr. Spectrosc. Res.*, 1992, **22**, 523–526.
3. G. F. Kröger and W. Freiberg, *Z. Chem.*, 1965, **5**, 381–382.
4. T. Zhang, C. Wang, S. Liu, J.-L. Wang and W. Lin, *J. Am. Chem. Soc.*, 2014, **136**, 273–281.
5. V. Gomez, J. Benet-Buchholz, E. Martin and J. R. Galan-Mascaros, *Eur. J. Inorg. Chem.*, 2014, **2014**, 3125–3132.
6. Y. Boland, B. Tinant, D. A. Safin, J. Marchand-Brynaert, R. Clerac and Y. Garcia, *CrystEngComm*, 2012, **14**, 8153–8155.
7. N. E. Good, G. D. Winget, W. Winter, T. N. Connolly, S. Izawa and R. M. M. Singh, *Biochemistry*, 1966, **5**, 467–477.
8. A. Kandegedara and D. B. Rorabacher, *Anal. Chem.*, 1999, **71**, 3140–3144.
9. H. E. Mash, Y.-P. Chin, L. Sigg, R. Hari and H. Xue, *Anal. Chem.*, 2003, **75**, 671–677.
10. C. J. M. van der Ham, F. Işık, T. W. G. M. Verhoeven, J. W. Niemantsverdriet and D. G. H. Hetterscheid, *Catal. Today*, 2017, **290**, 33–38.
11. D. A. Buttry and M. D. Ward, *Chem. Rev.*, 1992, **92**, 1355–1379.
12. A. J. Bard and L. R. Faulkner, *Electrochemical Methods: Fundamentals and Applications*, Wiley, New York, 2000.
13. R. Boulatov, J. P. Collman, I. M. Shiryaeva and C. J. Sunderland, *J. Am. Chem. Soc.*, 2002, **124**, 11923–11935.
14. M. S. Thorum, J. Yadav and A. A. Gewirth, *Angew. Chem. Int. Ed.*, 2009, **48**, 165–167.